INTERNATIONAL JOURNAL FOR NUMERICAL AND ANALYTICAL METHODS IN GEOMECHANICS
*Int. J. Numer. Anal. Meth. Geomech.*, **24,** 165–182 (2000)

# NEW BOUNDS FOR THE HEIGHT LIMIT OF A VERTICAL SLOPE

J. PASTOR*, T-H. THAI AND P. FRANCESCATO

*Laboratoire Matériaux Composites (LaMaCo), E.S.I.G.E.C., Université de Savoie, 73376 Le Bourget du Lac, France*

## SUMMARY

Using the finite element method, the static and kinematic methods of limit analysis provide tools to solve many stability problems in mechanics of continuous media. The classic problem of the height limit of a Tresca or Mises vertical slope subjected to the action of gravity stems naturally from this theory in plane strain. Although the exact solution to this problem remains unknown, the present work has produced precise bounds using the static and kinematic approaches conjointly: the height limit is now between 3·760 and 3·786 $C/\gamma$, $\gamma$ being the weight per unit volume and $C$ the soil cohesion. These tests also show that both methods, used on current workstations with industrial optimization codes such as XPRESS or OSL, are capable of solving any plane problem of limit loads in geotechnics or in structural calculus. Copyright © 2000 John Wiley & Sons, Ltd.

KEY WORDS: vertical slope; limit analysis; height limit bounds; finite element method; linear optimization

## 1. INTRODUCTION

### *1.1. Statement of the problem*

The problem under consideration is one of stability in the excavation of a vertical slope, a slope of sufficient length for the plane strain hypothesis to be admissible. This slope, of height $h$, is subjected only to its own weight (Figure 1). The constituent material, the soil, is homogeneous, isotropic, and of weight per unit volume $\gamma$. It obeys the Tresca plasticity criterion characterized by $C$ cohesion. Let us remind the reader that the Tresca and Mises criteria, identified in shearing, *coincide in plane strain.*

This is a classic problem of Limit Analysis or Yield Design theory.[1] Consequently, as seen below, the stability analysis of this structure involves determining the limit value $Q_{\lim}$ of the so-called loading parameter, defined here by the relation:

$$Q_\gamma = \frac{\gamma h}{C} \tag{1}$$

* Correspondence to: Professor J. Pastor, Laboratoire Matériaux Composites (LaMaCo), E.S.I.G.E.C., Université de Savoie, 73376 Le Bourget du Lac, France. E-mail: joseph.pastor@univ-savoie.fr

CCC 0363–9061/2000/020165–18$17.50

*Received 24 November 1998*
*Revised 26 April 1999*

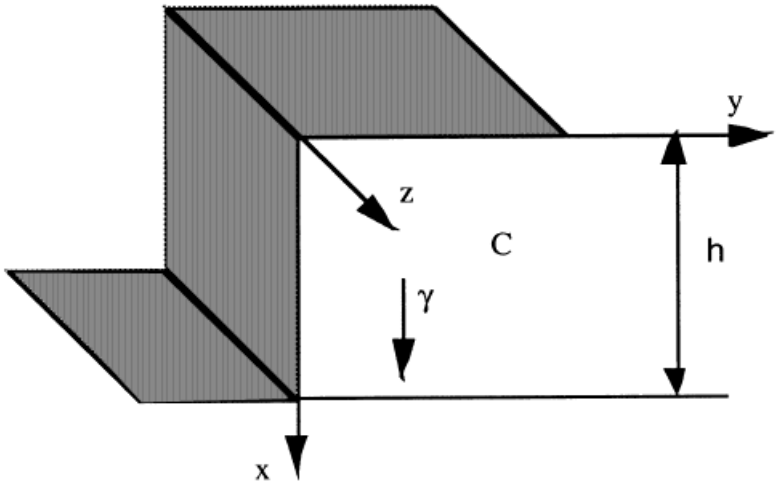


Figure 1. The vertical slope

and the associated kinematic parameter by

$$\dot{q}_\gamma = \frac{C}{h} \int_V u_x \, \mathrm{d}V \tag{2}$$

where $V$ designates the volume of a length of soil unit, $\boldsymbol{\sigma}$ and $\mathbf{u}$ being respectively, the stress and two-dimensional displacement velocity fields.

Several researchers have studied this classic problem. A precursor among those who have numerically treated the static method of limit analysis in geotechnics is Lysmer[2] who proposed a formulation where the unknowns were the stress vectors on the sides of each angle of the finite element P1, with the final problem coming under linear optimization. This method, recently adopted by Chuang,[3] was applicable to mechanical systems with bounded volume. Based on Lysmer's work, Pastor,[4] and Pastor and Turgeman[5] proposed a static method leading to improved numerical treatment, as Sloan[6] pointed out, but nevertheless viable for a mechanical system with bounded volume, as were the predecessors.

For semi-infinite problems such as those encountered with slopes, this restriction can lead to false solutions, as demonstrated by Pastor[7] *even if the mesh is bordered by a layer of large-dimension finite elements*. This drawback was eliminated by the same author in Reference 8 where the boundaries of the imperatively finite mesh were bordered with special or infinite elements (also called extended elements) provided with special conditions, e.g., *the stress fields remain admissible beyond the mesh*. These same elements were taken up in Reference 9 in the axially symmetric case, and used *identically* in a recent paper by Yu and Sloan.[10] Since 1978 the method has been extended to different anisotropic cases by Pastor,[11,12] Pastor and Turgeman,[13] Pastor *et al.*,[14,15] and within the domain of geotechnics, in the calculation of limit loadings of reinforced soils.[16,17]

With regard to both limit analysis methods, Anderheggen and Knöpfel[18] proposed a mixed formulation for bounded continua based on the linearization of the plasticity criterion. Fremond

 

and Salençon[19] solved the original kinematic problem for geotechnic problems using a non-linear optimization method. Following this work, Turgeman[20,21] proposed a kinematic method based on the linearization of the criterion, obtained independently of Capurso's[22] methods. In Turgeman's[21] work the discontinuity of velocity is allowed without any sign restriction, the kinematic result remaining a rigorous upper bound.[13] More recently, Abdi and Pastor[23] extended it to the case of reinforced soils treated by homogenization,[17] with Coulomb's soil as a special case. In both studies all inner edges of the finite element mesh were potential arbitrary discontinuities of displacement velocities, as in Reference 24 later.

Following Drucker and Prager's[25] treatment of Tresca or von Mises vertical slopes, ($Q_{\lim} \geqslant 2$), many authors set out to analytically or numerically construct stress fields leading to better lower bounds of $Q_{\lim}$. Heyman[26] reached $Q_{\lim} \geqslant 2{\cdot}73$ (the best purely analytical value) and Josselin de Jong[27] obtained $Q_{\lim} \geqslant 3{\cdot}39$ with a semi-analytical technique. The best value published to date was obtained by Pastor,[8] for a value of $Q_{\lim} \geqslant 3{\cdot}635$.

From the kinematic point of view now, using velocity fields by rotating blocks, Taylor[28] obtained $Q_{\lim} \leqslant 3{\cdot}831$. It is only recently that de Buhan *et al.*,[29] obtained $Q_{\lim} \leqslant 3{\cdot}817$. Finally, Bekaert,[30] based on a clever mechanism with several rigid rotating blocks, obtained $Q_{\lim} \leqslant 3{\cdot}793$. The time taken to improve Taylor's result, despite several intermediary attempts in the literature, is an indication of the difficulty posed by this problem of limit loading.

### *1.2. Theorems and methods of limit analysis*

Assume system $A$ of boundary $S$ and volume $V$, composed of rigid perfectly plastic and standard materials: the plasticity criterion $f(\boldsymbol{\sigma}) = 0$, convex, is also the strain rate potential. Moreover, the conditions at the defined boundaries in stress and displacement velocity on $S$ should allow the free plastic flow of $A$.

A stress field $\boldsymbol{\sigma}$ is admissible if it is:

(1) statically admissible (SA), i.e., the equilibrium equations, the possible stress continuities, and the boundary conditions are verified,
(2) plastically admissible (PA), i.e. $f(\boldsymbol{\sigma}) \leqslant 0$ at every point of $A$.

A strain rate field $v$ is admissible if it is:

(3) kinematically admissible (KA), i.e. $v$ is derived from a displacement velocity field $\mathbf{u}$ which satisfies the boundary conditions,
(4) plastically admissible (PA), i.e. $v$ satisfies the normality law:

$$\text{(i)}\ \ v = \lambda \frac{\partial f(\boldsymbol{\sigma})}{\partial \boldsymbol{\sigma}}, \quad f(\boldsymbol{\sigma}) = 0, \quad \lambda \geqslant 0 \ \text{(i.e. } \boldsymbol{\sigma} \text{ associated with } v) \tag{3}$$

(ii) the normality law is also verified for the possible velocity discontinuities.

If the theorem of virtual power can be written:

$$\int_V \boldsymbol{\sigma} : v \mathrm{d}V = \mathbf{Q}(\boldsymbol{\sigma}) \,.\, \dot{\mathbf{q}}(v) \tag{4}$$

where the $n$-vectors $\mathbf{Q}$ and $\dot{\mathbf{q}}$ are, respectively, the generalized forces and the velocities defined as linear applications on, respectively, $\{\boldsymbol{\sigma}\ \text{SA}\}$ and $\{v\ \text{CA}\}$ sets, then the mechanical system $A$ is subjected to a loading process with $n$ parameters.

 

A loading $\mathbf{Q}$ to which at least one admissible stress field $\boldsymbol{\sigma}$ can be associated, is said to be admissible, $K$, the convex set of admissible loadings of $\mathbf{R}^n$, is defined by

$$K = \{\mathbf{Q}(\boldsymbol{\sigma}), \text{ admissible } \boldsymbol{\sigma}\} \tag{5}$$

The numerical method applying the static theorem is detailed in section 2. In the case of a single loading parameter, as here, the static method leads to a lower bound of the loading limit $Q_{\lim}$.

Considering the fields of admissible strain rate, the kinematic theorem stipulates that the convex $K$ is obtained by the intersection of half-spaces $E(v)$ of $\mathbf{R}^n$ defined by

$$E(v) = \{\mathbf{Q}/\mathbf{Q}(\boldsymbol{\sigma})\cdot\dot{\mathbf{q}}(v) \leqslant P(v), \text{ admissible } v\}$$

$$P(v) = \int_V \pi(v)\,\mathrm{d}V, \tag{6}$$

$$\pi(v) = \boldsymbol{\sigma} : v, \boldsymbol{\sigma} \text{ associated with } v$$

where $P(v)$ is the dissipated power in $A$, with, if need be, the addition of the contribution of the discontinuity lines in displacement velocity. The resolution, for different directions of the given kinematic loading directions $\dot{\mathbf{q}}^{\mathrm{d}}$, of the problem:

$$P_{\min} = \mathrm{Min}\{P(v)/v \text{ admissible}, \dot{\mathbf{q}}(v) = \dot{\mathbf{q}}^{\mathrm{d}}\} \tag{7}$$

gives the family of hyperplans tangent to $K$ of equation $Q_i\dot{q}_i^{\mathrm{d}} = P_{\min}$; hence an approach to $K$ from the outside. The numerical method based on the kinematic theorem is detailed in section 3. In the case of slopes, the method leads to an upper bound in $Q_{\min}$ that will be denoted by $Q^+$ for simplicity. Salençon[1] provides a more detailed discussion on the theory of Limit Analysis and Yield Design theory.

## 2. THE STATIC APPROACH

The static problem in a non-bounded environment using the finite element method is detailed in Reference 8. The following is a brief reminder of the characteristics of the static program with a presentation of more recent features.

### *2.1. Description of the stress field* $\boldsymbol{\sigma}$

The mesh zone of the slope is divided into triangles. The variation of the stress field $\{\sigma\}$ is linear in $x$ and $y$ on the triangle and is written in a condensed form in numeric notation as follows:

$$\{\sigma^e\} = \sum_{p=1}^{3} \{a_p + b_p x + c_p y\}\{\sigma^p\} \tag{8}$$

where $\{\sigma^e\} = \{\sigma_x, \sigma_x, \tau_{xy}\}^{\mathrm{T}}$ represents a vector whose components are those of the stress tensor within the element, $\{\sigma^e\}$ equal $\{\sigma^p\}$ to the node $p$, and $a_p, b_p, c_p$ are the constants defined in Reference 31.

### *2.2. Conditions making* $\boldsymbol{\sigma}$ *statistically admissible* (*SA*)

(a) The indefinite equilibrium equations are written (positive compressions):

$$\sigma_{ij,j} = \gamma_i \tag{9}$$

 

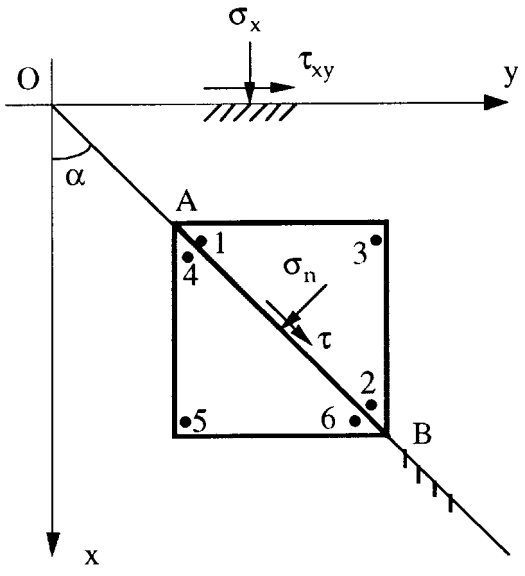


Figure 2. Continuity of $\sigma_n$ and $\tau$ between two adjacent triangles

where the non-zero component of $\gamma$, the weight per unit volume of the media, is considered as an additional variable to maximize and is thus the functional of the problem.

(b) The continuity of $\sigma_n$ and $\tau$ between two triangles (Figure 2) is imposed on points $A$ and $B$, which, given the linearity of $\{\sigma\}$, leads to its verification along $[AB]$. Note that the static method formulation allows stress discontinuities at all edges of two adjacent triangles. This kind of mesh is referred to, hence forth, as 'fully discontinuous' meshes.

The null stress boundary conditions are treated similarly by vanishing the normal and tangential stress at the concerned boundaries.

### 2.3. *Conditions making* $\boldsymbol{\sigma}$ *plastically admissible* (*PA*)

For the field $\boldsymbol{\sigma}$ to be PA, the plasticity criterion should be fully verified. In plane strain, the Tresca (or Mises) criterion is written:

$$f(\boldsymbol{\sigma}) = \sqrt{(\sigma_x - \sigma_y)^2 + 4\tau_{xy}^2} - 2C \leqslant 0 \tag{10}$$

As a result of the convexity of the criterion and of (8), the stress field $\{\sigma\}$ will be PA if it satisfies at each element's apex the following criterion linearized from the inside:

$$f_r(\boldsymbol{\sigma}) = (\sigma_x - \sigma_y)\cos\frac{2\pi r}{m} + 2\tau_{xy}\sin\frac{2\pi r}{m} - 2C\cos\frac{\pi}{m} < 0, \quad r = 1 \text{ to } m \tag{11}$$

where $m$ is greater than or equal to 3.

 

### *2.4. Extending conditions*

The extension of the stress field beyond the mesh zone is indispensable in making this field admissible everywhere within the semi-infinite medium. This problem is resolved for the Coulomb (and Tresca as a special case) criterion by using additional boundary elements which generate triangular or rectangular semi-infinite zones, which in turn allow the field to be extended in all directions beyond the mesh.[8] The field is admissible in these semi-infinite zones under the following conditions, in addition to those mentioned above:

(a) continuity of $\sigma_n$ and $\tau$ at the passage of a boundary line between zones,
(b) non-violation of the criterion beyond the generator element,

the indefinite equilibrium having been respected given the P1 character of the elements used.

All these conditions create a set of linear equations or inequations in the stress nodal unknowns $\{\sigma^e\}$. Given the linear nature of the functional, the problem results in a linear optimization problem.

### *2.5. Final numerical form of the static method*

As a result of the finite element discretization and the SA and PA conditions, the implementation of the lower bound static approach of Limit Analysis leads to the following linear programming problem ($P^-$):

$$(P^-)\begin{cases} \text{Max } F = \{c\}^{\mathrm{T}}\{X\} = \gamma \\ \text{with} \\ [A]\{X\} = \{B\} \\ [C]\{X\} \leqslant \{D\} \end{cases}$$

where $F$ is simply the variable $\gamma$. The solved problem is in fact a dual one in the LP sense: the LP codes are much more efficient for problems with many more columns than lines, as given below.

$$(P_{\text{dual}})\begin{cases} \text{Min } F = \{B\}^{\mathrm{T}}\{Y\} + \{D\}^{\mathrm{T}}\{Z\} \\ \text{with} \\ [A^{\mathrm{T}}C^{\mathrm{T}}]\begin{Bmatrix} Y \\ Z \end{Bmatrix} = \{c\} \\ \{Z\} \geqslant 0 \end{cases} \tag{12}$$

### *2.6. Results*

Each mesh is formed of segments at 0, 90 and $\pm 45^\circ$ in relation to $Ox$ and gives a value of $(\gamma h/C)_{\text{prol}}$. Several regular meshes were made and described in Reference 32. In each case, the optimal solutions were post-analysed so that the solution was rigorous to the precision level of the processor calculations. To date, the most powerful mesh includes 3232 Lagrange P1 triangles (Figure 3); its dual implementation leads to the resolution of the linear optimization problem of 29,089 lines and 957,432 columns (2,852,184 non-zero terms) and to the following result:

$$\frac{\gamma h}{C} \geqslant 3{\cdot}76037 \tag{13}$$

 

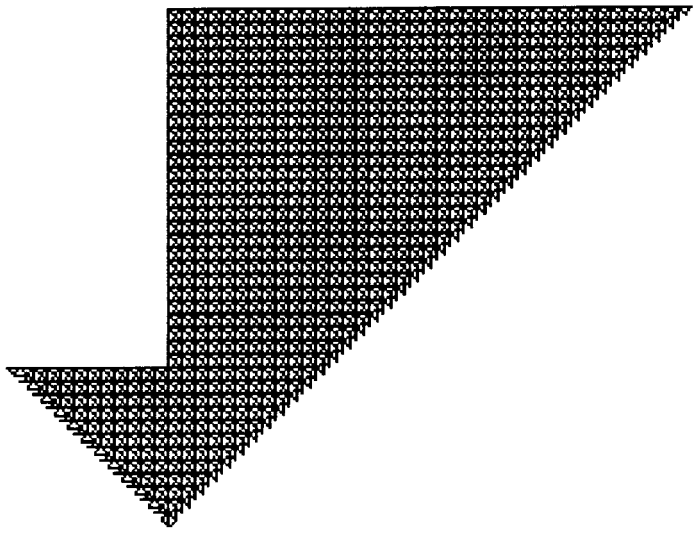

Figure 3. Mesh with $h = 27$ and $(\gamma h/C)_{\text{stat}} = 3{\cdot}76037$

Resolving this problem by the LP code called OSL[33] (Optimization Subroutine Library, IBM 1992) requires three weeks of calculations on a SUN-Ultra-2 workstation with an Ultra-Sparc 170 MHz processor with 192 MB of RAM. It should be pointed out here how efficient the current LP codes are, which brings limit analysis tools to a level of efficiency comparable to classical finite element codes. The possibility of saving intermediary bases, a very useful specification for treating LP problems, allows for risk-free processing over several weeks.

On the other hand, improving the efficiency of the method is not easy because, in general, our large weighting problems lead to numerical problem hard to solve, intentionally, by standard LP code for better user accessibility. Untill now XPRESS,[34] and especially OSL[33] have been very impressive, allowing us not to elaborate non-linear methods as in Reference 35. Note that recent industrial codes, which combines non-linear techniques and linear programming in the so-called Interior Point Methods, are available and will be tested with the present large (weighting) problems.

## 3. THE KINEMATIC APPROACH

The kinematic method (7) leads to minimization of the dissipated power over the set of admissible velocity fields. This problem is non-linear owing to the expression of this power. The following procedure is recommended for the use of standard optimization codes.

### *3.1. Description of the displacement velocity field*

Here the slope is also discretized in triangles for which each apex is affected by a two-component vector displacement $\{\delta\}$. For each triangle there is

$$\{\delta\} = \begin{Bmatrix} u_x^{(i)} \\ u_y^{(i)} \end{Bmatrix}, \quad i = 1\text{–}3 \tag{14}$$

 

The variation of the field **u** is linear in $x$ and $y$ on each triangle. The components of **u** are written in relation to the nodal displacement (14) with the definite classic interpolation functions in Reference 31, as in the static approach.

### 3.2. Linearization of the criterion

The Tresca (or Mises) criterion, here linearized *from the outside*, is expressed by

$$f_r(\boldsymbol{\sigma}) = (\sigma_x - \sigma_y)\cos\frac{2\pi r}{m} + 2\tau_{xy}\sin\frac{2\pi r}{m} - 2C \leqslant 0, \quad r = 1 \text{ to } m \tag{15}$$

where $m$, a linearization parameter, is greater than or equal to 3.

Note that similar kinematic formulation was also applied to the vertical slope stability problem with Coulomb reinforced material.[17]

### 3.3. Conditions making the strain rate field admissible

The kinematic theorem requires that the strain field be both KA and PA (and thus admissible) at every point of the structure. Let us consider the discretized structure in a mesh of NT triangles denoted by $e_k$, for which each side is a line of potential discontinuity in displacement velocity (Figure 4).

Note $v$ as the displacement velocity tensor at any point $M$ of $e_k$. The component of $v$ are expressed by (positive compression):

$$v_{ij} = -\frac{1}{2}(u_{i,j} + u_{j,i}) \tag{16}$$

The displacement velocity field derived from $\mathbf{u}^{(M)}$ is thus constant on the element $e_k$ and is expressed linearly in relation to the nodal variables by appropriate derivation of the interpolation functions.

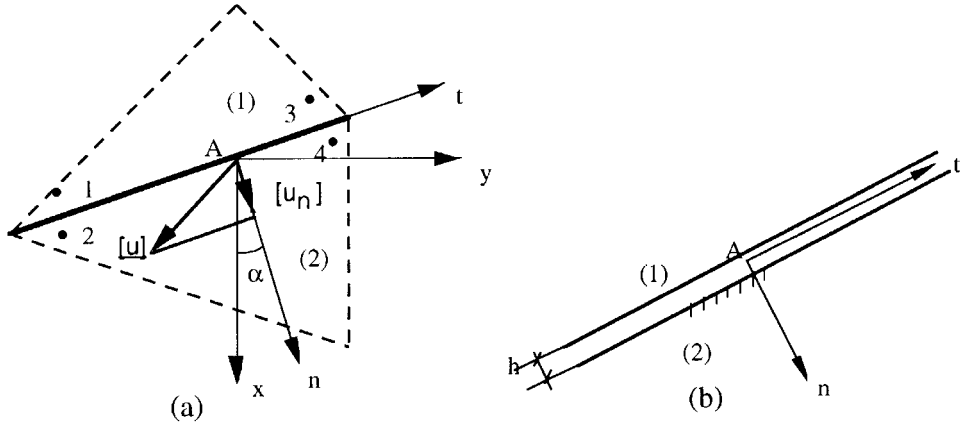


Figure 4. Displacement velocity discontinuity segment

 

The boundary conditions in displacement velocity will be satisfied by cancelling the components of a fictional node associated with the boundary of the mesh, a potential discontinuity line. The loading condition $\dot{\mathbf{q}}(v) = \dot{\mathbf{q}}_\gamma = \dot{\mathbf{q}}^{\mathrm{d}}$ is naturally linear.

In addition, the strain rate field is PA if it satisfies the law of normality (3); it is admissible if it is also KA. The equality between relations (3) and (16) must therefore be written on each element, which brings three linear equations, for each element $e_k$, to the nodal displacements $u_x^k$ and $u_y^k$ and to the plastic coefficients $\lambda_r^k$, new unknowns of the problem.

### *3.4. Discontinuity lines in displacement velocity*

The numerical implementation of the kinematic method is only efficient if it authorizes the development of at least one rigid block mechanism,[13,20] because of the highly constraining character of the PA condition required for the velocity field. However, all the tests carried out since in the literature have proved ineffectual for this problem. It is for this reason that we have chosen to use very refined 'fully discontinuous' meshes, i.e. meshes which systematically present a segment of discontinuity, written $S_k$, to the interface of two adjacent finite elements. The admissible character of the displacement velocity field therefore implies that additional relations are required: conditions that will be defined below. Upper bounds techniques associated with 'fully discontinuous' meshes are very efficient for solving general geotechnical yield design problems as discussed in References 17, and 23 and 24.

At a point $A$ of the segment $S_k$ an orthonormal reference point is defined $(A, \mathbf{n}, \mathbf{t})$ where $\mathbf{n}$ is the normal in $A$ (Figure 4). In this reference point, the velocity discontinuity components $[\mathbf{u}]$ are expressed by $[u_n] = u_n^{(1)} - u_n^{(2)}$ and $[u_t] = u_t^{(1)} - u_t^{(2)}$ where (1) and (2) represent the two zones separated by the segment $S_k$.

The boundaries of the plasticity domain in the Mohr plane (Figure 5), written $G(\boldsymbol{\sigma}) = G(\sigma_n, \tau)$ are defined by

$$G(\boldsymbol{\sigma}) = |\tau| - C \leqslant 0 \tag{17}$$

This boundary is naturally linear (Figure 5).

The rule of normality requires that the function $G(\boldsymbol{\sigma})$ be a potential function of the discontinuity $[\mathbf{u}]$, let us say:

$$[\mathbf{u}]\ \mathrm{PA} \ \Leftrightarrow \begin{cases} \exists\ \boldsymbol{\sigma} = (\sigma_n, \tau) & \text{with } G(\boldsymbol{\sigma}) = 0 \\ [\mathbf{u}] = \xi \dfrac{\partial G(\boldsymbol{\sigma})}{\partial \boldsymbol{\sigma}}, & \xi \geqslant 0 \end{cases} \tag{18}$$

Each discontinuity line includes two facing node couples located at the extremities of $S_k$ (Figure 4), couples which are denoted by I (nodes 1 and 2) and II (nodes 3 and 4) and in which plastically admissible conditions are obtained as

$$[u_n]^i = 0, \quad [u_t]^i = \xi_1^i - \xi_2^i, \quad \xi_j^i \geqslant 0, \quad i = \mathrm{I}, \mathrm{II}, \quad j = 1, 2 \tag{19}$$

The components of the velocity discontinuity vector $[\mathbf{u}]$ in each node couple I and II of a segment $S_k$ are also expressed in the reference point $(A, \boldsymbol{e}_x, \boldsymbol{e}_y)$ with the angle $\alpha$ and the nodal displacements $u_x^k$ and $u_y^k$. Taking into account the linearity of $[\mathbf{u}]$ along $S_k$, one needs only to impose the conditions of (19) to the extremity nodes for the admissible character of $[\mathbf{u}]$ to be verified all along $S_k$.

 

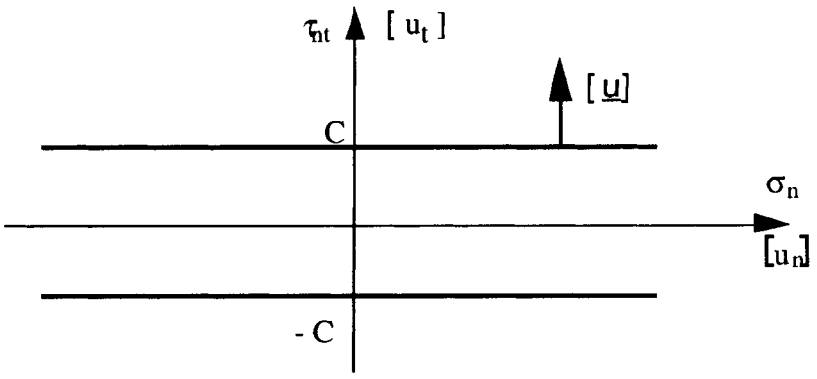


Figure 5. TRESCA (or MISES) criterion in the Mohr plane

### 3.5. *Application of the theorem of virtual power*

In plane strain, the dissipated power $P(v)$ is divided into a first part dissipated in the volume $V$ (here $S$), and second part dissipated along the line $l$ of displacement velocity discontinuity:

$$P(v) = \int_S \pi(v)\,\mathrm{d}S + \int_{\cup l} \pi([\mathbf{u}])\,\mathrm{d}l \tag{20}$$

The power dissipated by unit of volume function then becomes (15) and the admissibility conditions of $v$, the criterion being equal to zero (Capurso[22], Turgeman[20]):

$$\pi(v) = \mathrm{Min}_\lambda \left\{ 2C \sum_{r=1}^{n} \lambda_r \right\} \tag{21}$$

Similarly, the dissipated power by unit of length function along $S_k$ under the conditions of (17) and (19) becomes

$$\pi([\mathbf{u}]) = \mathrm{Min}_\xi C(\xi_1 + \xi_2) \tag{22}$$

The functional to optimize is the total dissipated power in the structure discretized in triangular finite structures (of the Lagrange P1 type). In the present case the minimized functional is the upper bound of the dissipated power defined by the right-hand side of (23):

$$P(v) \leqslant \mathrm{Min}_{\lambda,\xi} C \left\{ \sum_{k=1}^{NT} \left( \sum_{r=1}^{n} 2\lambda_r^k \right) S_k + \sum_{k=1}^{\mathrm{NDISC}} \left( \sum_{i=1}^{4} \frac{1}{2}\,\xi_i^k \right) l_k \right\} \tag{23}$$

where $s_k$ is the surface of the element $S_k$ (in NT quantities) and $l_k$ is the length of the $k$th segment of discontinuity (in NDISC numbers). In fact, this upper bound character is linked to the integration along the sides of the discontinuities where theoretically the velocity discontinuity could change signs.[21] In practice, this case never comes up and (23) can be considered as an equality.

### 3.6. *Final numerical form of the kinematic method*

The minimization of the second member subject to the constraints of (3) and (19), to which must be added the boundary conditions in $\mathbf{u}$ and the condition $\dot{\mathbf{q}}(v) = \dot{\mathbf{q}}_\gamma = \dot{\mathbf{q}}^{\mathrm{d}}$, gives an upper bound of

 

the result by solving the linear optimization problem $(P^+)$:

$$(P^+)\begin{cases}\text{Min}\{F(\lambda,\xi)\}\\ \text{under}\\ [D].\{u\}=\{E\}\end{cases} \tag{24}$$

where $F(\lambda, \xi)$ is the functional formed by the unknown plastic multipliers, $\{u\}$ represents the vector formed by the components of the displacement velocities at the apices of the triangles and $[D]\{u\} = \{E\}$ is the system of linear equations expressing the KA and PA conditions of the velocity field $\mathbf{u}$ as well as the condition $\dot{\mathbf{q}}(v) = \dot{\mathbf{q}}_\gamma = \dot{\mathbf{q}}^{\mathrm{d}}$.

## 4. NUMERICAL RESULTS

### *4.1. Optimization of the mesh by the gradient method*

The methods described above are efficient provided that sufficiently refined meshes are used. This is the origin of the idea of a numerical optimization of the mesh to obtain 'the optimal positions' of nodal points by numerically calculating the partial derivatives of the functional and deducing the directions favourable to the displacement of these nodal points.

This method, detailed in Reference 36, was tested on a mesh of 288 elements and 865 nodes (Figure 6) which, in its initial configuration, provided an upper bound of $Q_\gamma$ equal to 3·818. After 14 iterations, the kinematic boundary stabilized at a value of 3·805. The evolution of the mesh demonstrated a slight modification of the discontinuity line separating the mesh zone from the rigid zone, essentially at the foot of slope (Figure 6). This value was again improved when the preceding mesh was transformed by dividing each element into four, increasing the number to 1152. This new mesh led to a new value of the upper bound equal to 3·797, an excellent value indeed.

This method would therefore seem efficient but its use still remains too time-consuming, at least today. This explains our use of another more intuitive method to obtain the desired meshes.

### *4.2. Meshes used and influence of the parameters*

Since the Coulomb prism gave an upper bound value equal to 4, many authors have approached this problem from a kinematic point of view, attempting to find the optimal form of the discontinuity line separating the mobile block from the rest of the body. Bekaert's[30] kinematic value was obtained with a mechanism of rotating blocks numerically optimized in 15 circles.

The best meshes draw their inspiration from the mechanism developed by Bekaert. The zone set out by this mechanism is divided into horizontal and vertical bands whose respective widths $x_n$ and $y_n$ are in arithmetic progression so as to make the discretization at the foot of the slope denser (Figure 7). For a fixed height $h$ of the slope, the optimal reasons for using $x_n$ and $y_n$ the very refined meshes are obtained numerically from a pilot mesh (Table I).

The higher the number of planes linearizing the criterion, the more precise the kinematic estimation will be. It is shown, as expected, that the kinematic value obtained for a given mesh increases very little beyond 96 linearizing planes (see Figure 8 and Table II). The kinematic value will be obtained by associating an 'optimal' value of this number equal to 48 with a mesh, a reasonable CPU performance-time compromise.

 

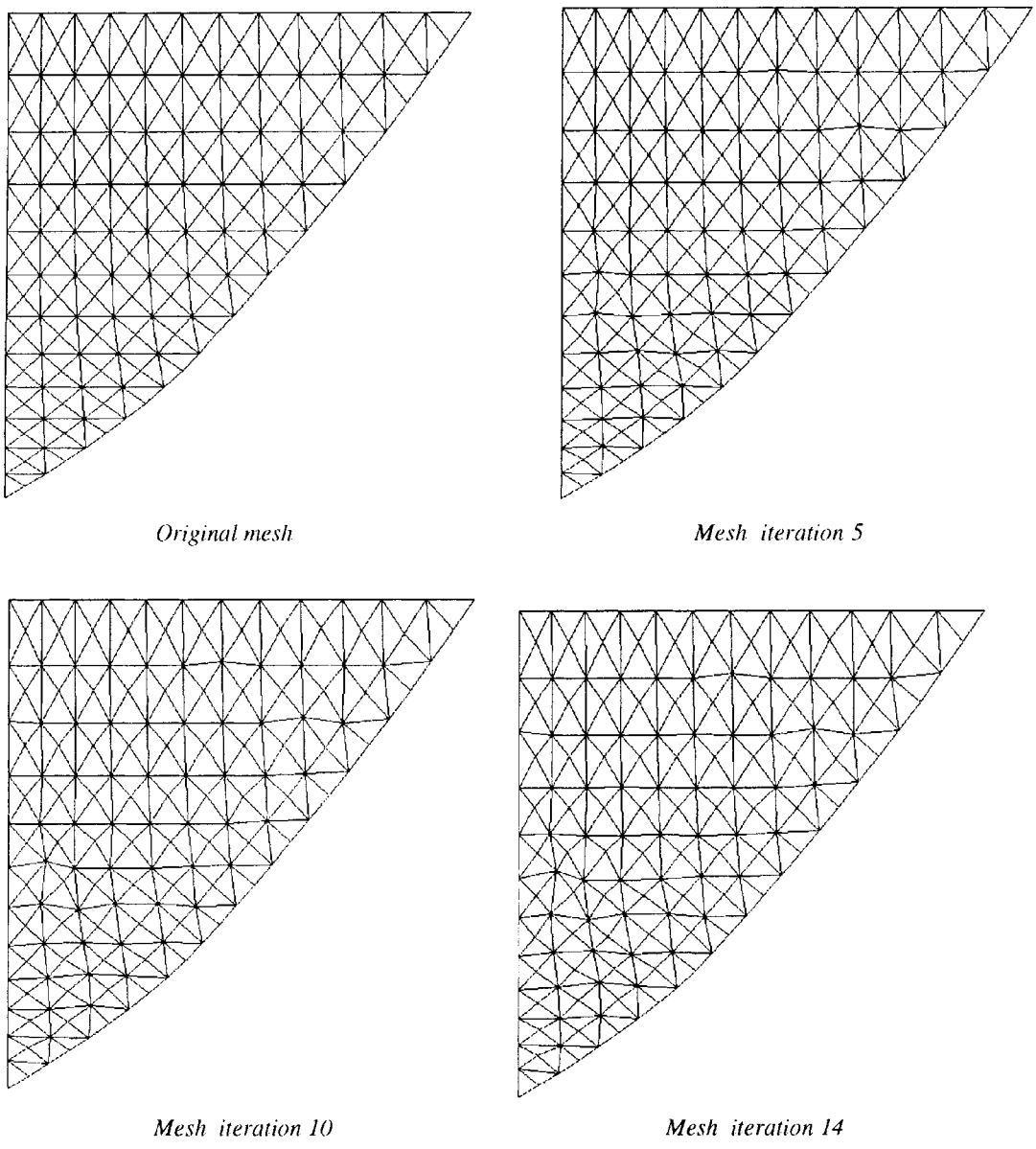


Figure 6. Evolution of a 288-element mesh obtained by the gradient method ($h = 12$)

### *4.3. Kinematic results*

The final problem is the one of linear optimization which is resolved with the OSL[33] code, installed on SUN workstations. The optimal displacement velocity fields **u** are then obtained. Finally, these fields are analysed using totally independent post-treatment procedures so that

 

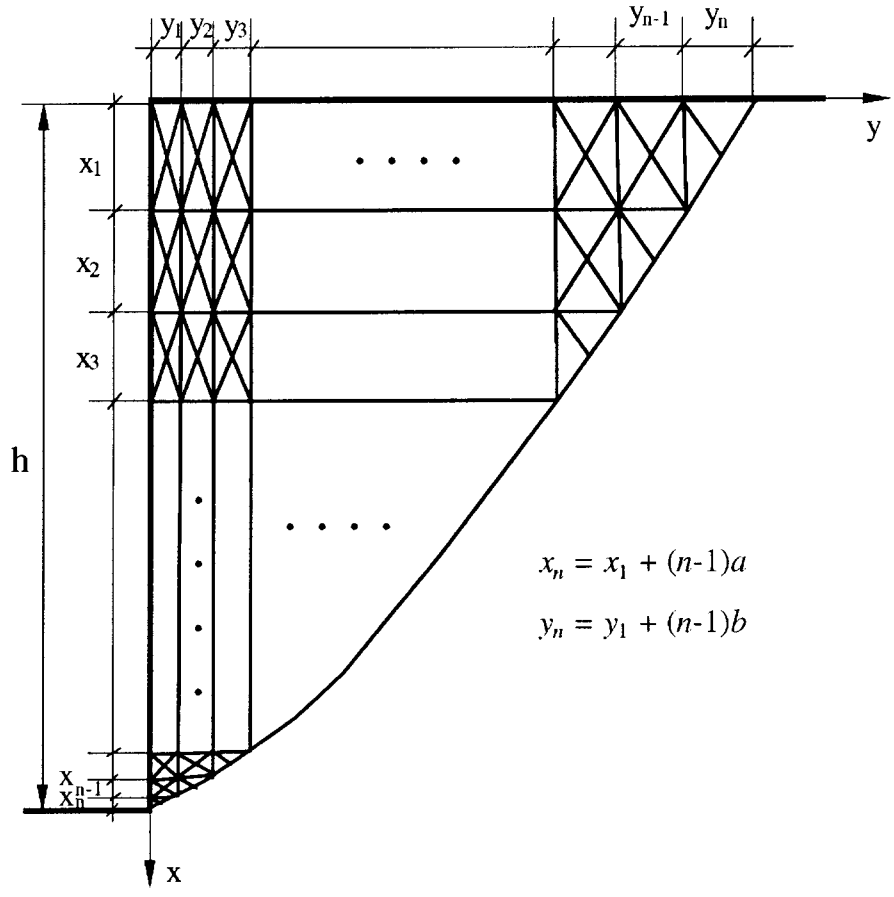


Figure 7. Principle of the meshes used

Table I. Optimal reasons $a$ and $b$ obtained for different heights $h$

| $h$ | 6 | 12 | 18 | 24 | 30 | 36 | 42 |
|---|---|---|---|---|---|---|---|
| $a$ | − 2·450 | − 1·550 | − 1·033 | − 0·775 | − 0·620 | − 0·517 | − 0·438 |
| $b$ | 1·500 | 0·750 | 0·500 | 0·375 | 0·300 | 0·250 | 0·225 |

their admissible character is only limited by the precision level of the computer calculations. These analyses verify *a posteriori* the admissibility conditions of fields in the volume and along the discontinuity lines by a direct calculation using optimal **u** fields. Similar procedures are used as indicated earlier in this paper in order to verify the admissible character of stress fields as a solution to the static problem.

 

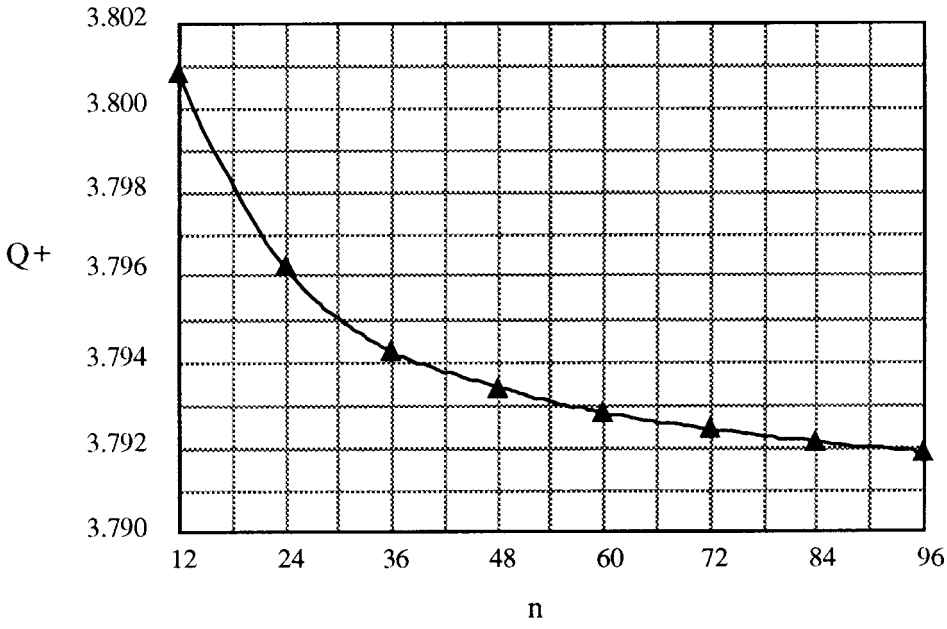


Figure 8. Evolution of parameter $Q^+$ in relation to the number of planes linearizing the criterion. A 1152-element mesh ($h = 24$)

Table II. Kinematic values $Q^+$ in relation to $n$. A 1152-element mesh ($h = 24$)

| $n$ | 12 | 24 | 36 | 48 | 60 | 72 | 84 | 96 |
|---|---|---|---|---|---|---|---|---|
| $Q^+$ | 3·80081 | 3·79620 | 3·79421 | 3·79339 | 3·79279 | 3·79240 | 3·79210 | 3·79185 |

This post-analysis is also capable of calculating the value of the exact power dissipated in the field **u** using the non-linearized criterion and analytic expressions of different powers. Thus, this work is used to calculate a new rigorous value of the loading parameter $Q = \gamma h/C$, said to be post-analysed and written $Q^*_{\text{post}}$. The latter is in general slightly below the optimal value on account of the outside linearization of the criterion.

Table III and Figure 9 give an idea of the evolution of the kinematic value $Q^+$ in relation to the refinement of the mesh used, the refinement being parametered by the height $h$ which gives the number of elements on the vertical facing of the slope. This refinement is a noticeable improvement; hence the pertinence of the form adopted for the mesh. Table III gives the sizes of the numerical problems and the CPU time required for resolving these problems, including matrix generation of stresses.

Observing the failure mode with the deformed mesh plotting obtained for the best kinematic value (Figure 10), it becomes clear that the strain is concentrated especially at the foot of the slope and along the discontinuity line separating the rigid zone from the meshed section. Actually, the calculation of dissipated power after resolution shows that the dissipated power in the

 

Table III. Kinematic values of $Q^+$ and $Q^+_{post}$ obtained for different heights $h$. Characteristics of associated numerical problems

| $h$ | 6 | 12 | 18 | 24 | 30 | 36 | 42 |
|---|---|---|---|---|---|---|---|
| $Q^+$ | 3·835437 | 3·805585 | 3·797203 | 3·793391 | 3·791016 | 3·789132 | 3·788035 |
| $Q^+_{post}$ | 3·834987 | 3·804778 | 3·796194 | 3·792139 | 3·788489 | 3·786743 | 3·785864 |
| Matrix size | 649 × 4322 | 2593 × 17 282 | 5833 × 38 922 | 10 369 × 69 122 | 16 201 × 97 202 | 23 329 × 155 522 | 31 753 × 211 682 |
| CPU times | 20 (s) | 15 (mm) | 3 (h) | 24 (h) | 170 (h) | 700 (h) | 1000 (h) |

*on SUN Sparc 10–51 workstations

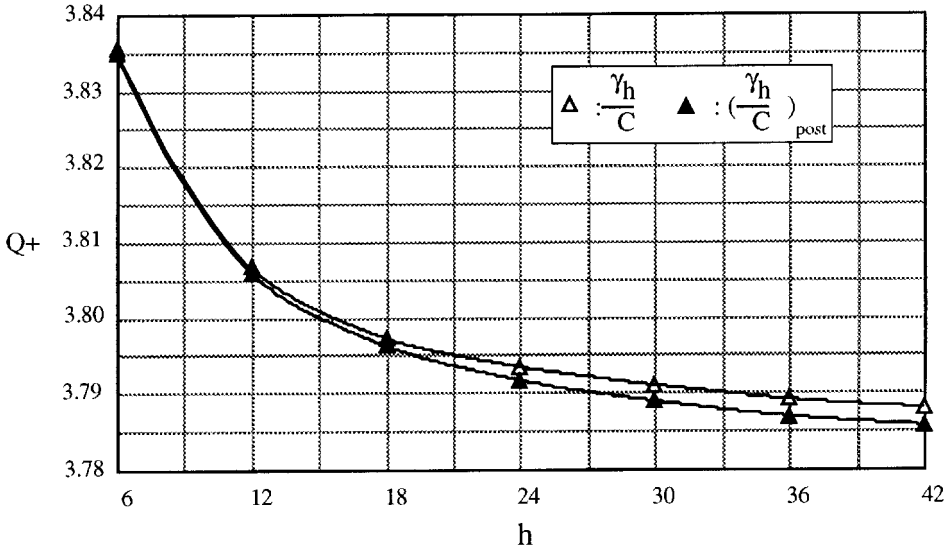


Figure 9. Variation of the parameter $Q^+$ in relation to $h$

discontinuity lines is roughly three times stronger than the volume power. The best kinematic value that we have obtained to date is finally:

$$Q^+ = 3{\cdot}785864$$

## 5. CONCLUSION

We were able to improve the kinematic and static values of the loading parameter of the vertical slope subjected to its own weight and thus obtain new bounds of the non-dimensional loading parameter $Q_\gamma = \gamma h/C$ as

$$3{\cdot}7603 \leqslant \frac{\gamma h}{C} \leqslant 3{\cdot}7859$$

 

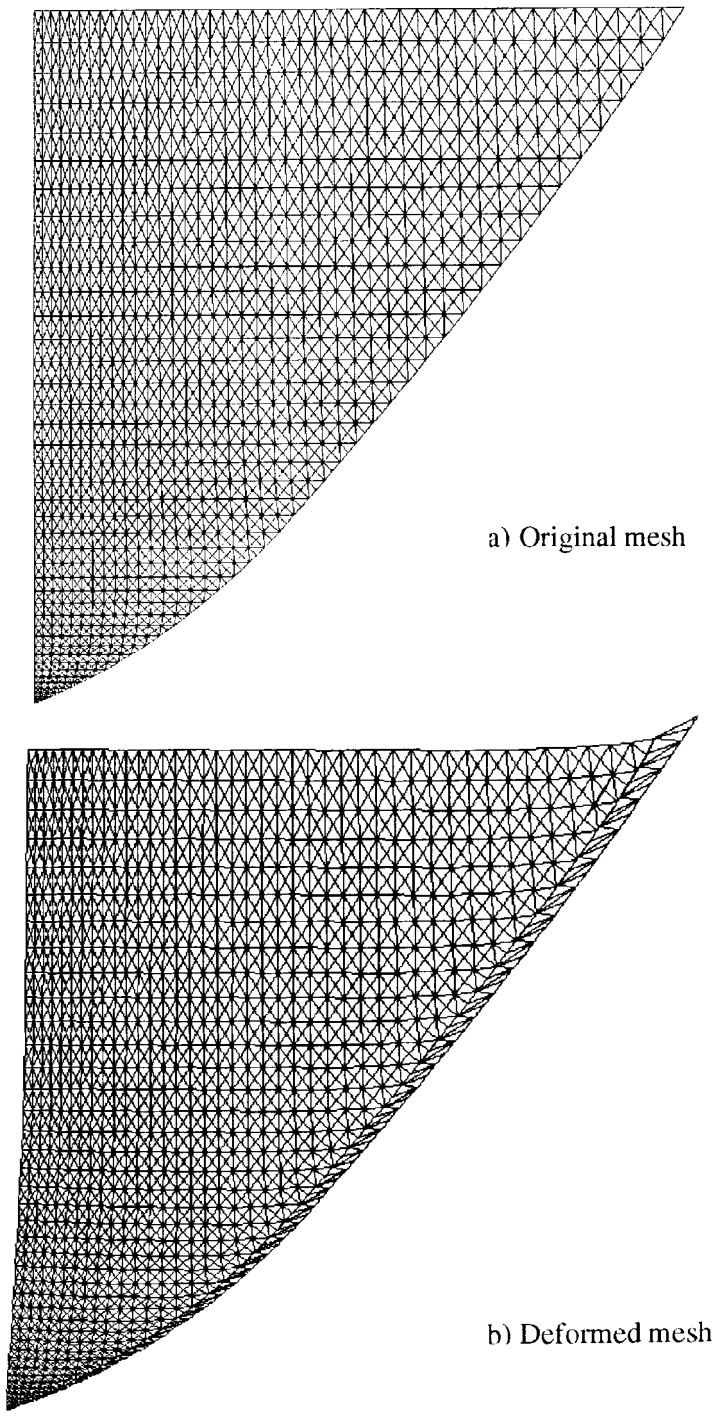


Figure 10. Initial and strained meshes, $h = 42$

 

The slight static-kinematic gap confirms the efficiency of the methods used in these problems of stability in the vertical slope; methods which gave both *rigorous and verifiable* results *a posteriori*. Moreover, this difficult slope problem particularly demonstrates the power of Limit Analysis methods in these stability problems, among others. This case is itself fundamental, but is also essential as a means of verification for other approaches of the elastoplastic type, demonstrating the advantage of obtaining the exact solution and so continuing the work presented herein. In support of the methods proposed, it should be noted that this type of problem cannot be appropriately treated with an industrial finite element code, because here the loading is of the integral type *and the discontinuities are indispensable*. Furthermore, the results of industrial codes, assuming they are obtained, cannot be interpreted in terms of bounds, even for a *very refined* mesh, in particular statistically. Finally, note the ability of this method to predict, through an approach analogous to Gurson's, the plasticity criterion of heterogeneous material,[37] as well as reinforced Coulomb soils.[17]

## REFERENCES


1. J. Salençon, *Calcul à la rupture et analyse limite*, Presses de l'ENPC, Paris, 1983.
2. J. Lysmer, 'Limit analysis of plane problems in soil mechanics', J. Soil Mech. Found. Div., ASCE **96** (SM4); *Proc. Paper* 7416, 1970, pp. 1311–1334.
3. P. H. Chuang, 'Stability analysis in geomechanics by linear programming, part I-II', *J. of Geotech. Engng*., **118,** 1696–1726 (1992).
4. J. Pastor, 'Application de l'analyse limite à l'étude de la stabilité des pentes et des talus', *Thesis*, USMG, Grenoble, 1976.
5. J. Pastor and S. Turgeman, 'Mise en œuvre numérique des méthodes de l'Analyse Limite pour les matériaux de von Mises et de Coulomb standards en déformation plane', *Mech. Res., Comm*., **3,** 469–476 (1976).
6. S. W. Sloan, 'Lower bound limit analysis using finite elements and linear programming', *Int. J. Numer. Anal. Meth. Geomech*., **12,** 61–77 (1988).
7. J. Pastor, Discussion "Limit Analysis of geotechnical problems by applying lower-bound theorem" by K. Araï et K. Tagyo, *Soils And Foundations*, **26,** 150–152 (1986).
8. J. Pastor, 'Analyse limite: détermination numérique de solutions statiques complètes. Application au talus vertical', *J. Méc. Appl*. (now *Eur. Jl. Mech.-A/Solids*), **2,** 167–196 (1978).
9. J. Pastor and S. Turgeman, 'Limit analysis in axisymmetrical problems: numerical determination of complete statical solutions', *Int. J. Mech. Sci*., **24,** 95–117 (1982).
10. H. S. Yu and S. W. Sloan, 'Upper bound limit analysis of a rigid-plastic body with frictional interfaces', *Int. J. Mech. Sci*., **36,** 219–229 (1994).
11. J. Pastor, 'Analyse limite et stabilité des fouilles' *X^e congrés international de Mécanique des sols et des travaux de Fondation*, *Proc. X-ICSMFE*, Balkema, Rotterdam, 1981.
12. J. Pastor, 'Application de la théorie de l'analyse limite aux milieux isotropes et orthotropes de révolution', *Thesis*, U.S.M.G. et I.N.P.G., Grenoble, 1983.
13. J. Pastor and S. Turgeman, 'Approches numériques des charges limites pour un matériau orthotrope de révolution en déformation plane', *J. de Mécanique Théorique et Appliquée*, (now *Eur. Jl Mech.-A/Solids*), **2,** 393–416 (1983).
14. J. Pastor, S. Turgeman and C. Avallet, 'Predicting the phenomenon of burying through gravity in purely cohesive sedimentary sea-beds', *Géotechnique*, **39,** 625–639 (1989).
15. J. Pastor, S. Turgeman and J.P. Boehler, 'Solution of anisotropic plasticity problems by using associated isotropic problems', *Int. J. Plasticity*, **6,** 143–168 (1990).
16. J. Pastor and R. Abdi, 'Analyse Limite et Homogénéisation: approche numérique', *9ème Congrès Français de Mécanique*, Metz, 1989.
17. R. Abdi, P. de Buhan, and J. Pastor, 'Calculation of the critical height of a homogenized reinforced soil wall: a numerical approach', *Int. J. Numer. Anal. Meth. Geomech*., **18,** 485–505 (1994).
18. E. Anderheggen and H. Knöpfel, 'Finite element limit anlaysis using linear programming', *Int. J. Solids Struct*., **8,** 1413–1431 (1972).
19. M. Fremond and J. Salençon, 'Limit analysis by finite-element methods', in A. C. Palmen (ed.), *Proc. Symp. on Role of Plasticity in Soil Mech*., Cambridge, England, 1973.
20. S. Turgeman, 'Etude des fondations sollicitées à l'arrachement par la théorie de l'analyse limite', *Thesis*, Université de Grenoble, 1976.


 

21. S. Turgeman, 'Contribution au calcul des charges limites en milieux isotropes et orthotropes de révolution par une approche cinématique numérique', *Thesis* U.S.M.G. and I.N.P.G., Grenoble, 1983.
22. M. Capurso 'Limit analysis of continuous media with piecewise linear yield condition', *Meccanica*, **6,** 53–58 (1971).
23. R. Abdi and J. Pastor, 'Charges limites de structures en sols renforcés', in J.P. Boehler and A.S. Khan, *Proc. 3rd Int. Symp. on Plasticity and Its Current Applications*, Plasticity '91 Grenoble, Elsevier, Amsterdam, 1991.
24. S. W. Sloan and P. W. Kleeman, 'Upper bound limit analysis with discontinuous velocity fields', *Comput. Meth. Appl. Mech. Engng.*, **127,** 293–314 (1995).
25. D. C. Drucker and W. Prager, 'Soil mechanics and plastic analysis or limit design', *Quart. Appl. Math.*, **10,** 157–165 (1952).
26. J. Heyman, 'The stability of a vertical cut', *Int. J. Mech. Sci.*, **11,** 845–854 (1973).
27. G. Josselin de Jong, 'Improvement of the lowerbound for the vertical cut off in a cohesive frictionless soil', *Géotechnique*, **28,** 197–201 (1978).
28. D. W. Taylor, *Fundamentals of Soil Mechanics*, Wiley, New York, 1948.
29. P. de Buhan, L. Dormieux and S. Maghous, 'Stabilité d'un talus vertical: amélioration de la borne cinématique', *C.R.Acad.Sci.*, **317 II,** 13–136 (1993).
30. A. Bekaert, 'Improvement of the kinematic bound for the stability of a vertical cut-off', *Mech. Res. Commun.*, **22,** 533–540, (1995).
31. O. C. Zienkiewicz, *The Finite Element Method*, 3rd edn, McGraw-Hill, New York, 1977.
32. J. Pastor, 'Analyse limite et talus vertical de Tresca: suite et (presque) fin', *Invited Conf. Journées de Mécanique et Ingénierie*, Sfax, Tunisie, 1996.
33. OSL, *Optimisation Subroutine Library*, IBM Corporation, Kingston, USA, 1992.
34. XPRESS-MP, Dash Associates, Blisworth, Northants NN7 3BX, 1992.
35. A. V. Lyamin and S. W. Sloan, 'A comparison of linear and non linear programming formulations for lower bound analysis', Piteruszczak and Pande (eds), *Numerical Models in Geomechanics*, Balkema, Rotterdam, 1997.
36. T. H. Thai, 'Analyse Limite: Application aux structures et aux matériaux poreux', *Thesis*, Université de Savoie, 1997.
37. P. Francescato and J. Pastor, 'Limit Analysis and Homogenization: predicting limit loads of periodic heterogeneous materials', *Eur. J. Mech., A/Solids*, **16,** 235–253 (1997).

 